Self-seeding of SASE-soft-X-ray FEL using artificial Bragg reflectors

Jean-Michel André, Philippe Jonnard, Olivier Peyrusse

Self-seeding of SASE-soft-X-ray FEL using artificial Bragg reflectors

Jean-Michel André[1], Philippe Jonnard[1], Olivier Peyrusse[2]

(1) Sorbonne Université, Faculté des Sciences et Ingénierie, UMR CNRS, Laboratoire de Chimie Physique – Matière et Rayonnement, 4 Place Jussieu, F-75252 Paris Cedex 05, France
(2) Aix-Marseille Université, CNRS UMR 7345, PIIM Marseille, France

Abstract

The use of artificial Bragg reflectors in double-crystal non-dispersive configuration and backscattering geometry is proposed to achieve the self-seeding of SASE-soft-X-ray FEL. It is shown that the proposed system verifies the set of criteria given by J. Feldhaus *et al.* [Opt. Commun. **140**, 341 (1997)]. Owing to the short duration of the x-ray pulses, the problem of reflection and self-seeding is discussed in the time-domain.

1. Introduction

Although the self-amplified spontaneous emission – x-ray free electron lasers (SASE-XFEL) are very effective, the stochastic starting-up process from electron beam shot noise leads to some problems as poor longitudinal coherence and broad, noisy spectrum. In order to improve the performances of SASE-XFEL in terms of coherence and spectral purity, self-seeding has been proposed and successfully tested under various schemes [1–4].

The self-seeding method uses an upstream XFEL coming from a first ondulator (modulator) working in the SASE linear regime. The pulse coming from the modulator is then put through an x-ray monochromator to generate a quasi-monochromatic radiation seeding for the downstream ondulator (radiator) which amplifies, in the non-linear regime, the seed to give coherent radiation with a narrow spectral bandwidth.

For hard x-rays, self-seeding is produced by filtering the SASE-XFEL radiation coming from the modulator by use of a thin crystal in transmission geometry ; this method has been successfully implemented for instance at LCSL [5]. In soft-x-ray and X-UV ranges,

self-seeding is generally obtained by monochromatizing the SASE-XFEL radiation by means of a diffraction grating and a system of mirrors and slits [1] (see figure 1). The main drawbacks of this operation mode are high cost since expensive variable line spacing gratings are generally used and low efficiency resulting from the moderate diffractive efficiency of the diffraction gratings (less than 20 %) and mirrors in this spectral range.

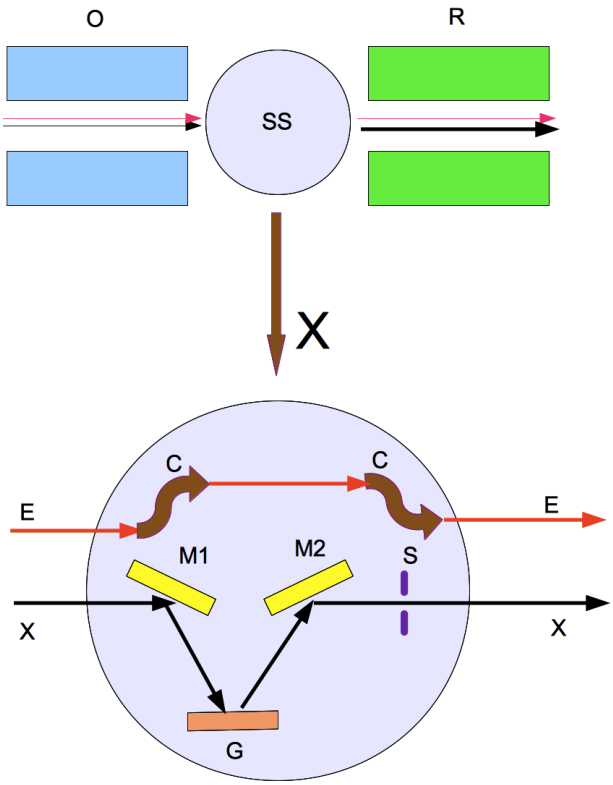

Figure 1 : Standard scheme of self-seeding (SS) for a soft-x-ray FEL ; monochomatization is performed by means of diffraction grating (G) mirrors (M) and slits (S). The first ondulator (O) is the modulator and the second one the radiator (R). The regime of O is linear while R ensures the amplification until saturation in a non-linear regime. X denotes the path of the x-ray beam while E denotes the path of the electron beam through the chicanes C.

In this paper we consider the problem of self-seeding in the soft x-ray range. We suggest the use of artificial Bragg reflectors which offer large reflectivity with respect to diffraction gratings at a relatively low cost. In section 2, we propose a layout based on double-crystal configuration equipped with multilayer Bragg reflectors in the backscattering geometry and discuss in section 3 the possibility of our proposal with respect to the criteria proposed by Feldhaus *et al.* in [1], for achieving self-seeding. Indeed the authors of [1] proposed in this reference, a set of criteria summed up in their

equation (6) which they consider necessary to satisfy in order to ensure lasing. For the sake of consistency, we give the formulation of the criteria relative to the self-seeding device SSD acting as a monochromator m:

- achieving a sufficient resolution $\mathcal{R}_m$ of the SSD, that is :

$$K_s \equiv \frac{\mathcal{R}_m}{\mathcal{R}_{SASE}} \ll 1 \tag{1}$$

where $\mathcal{R}_{SASE} \equiv \frac{\Delta\lambda}{\lambda}\Big)_{SASE}$ is the relative radiation bandwidth in terms of wavelength of the SASE-XFEL radiation at the exit of the modulator and $\mathcal{R}_m \equiv \frac{\Delta\lambda}{\lambda}\Big)_m$ the resolution of the SSD. In addition, a lower limitation concerning $\mathcal{R}_m$ is required, due to the fact that the length of the longitudinal coherence of the radiation cannot be larger that the length of the electron bunch σ_z, that is :

$$\frac{\lambda}{\pi\,\sigma_z} \leq \mathcal{R}_m \tag{2}$$

- achieving a sufficient transmission factor T_m of the SSD, defined as the product of the coefficient K_s with the integral global reflectivity R_m of the SSD, that is :

$$\frac{P_{in}^{(2)}}{P_{shot}} = G^{(1)}\,T_m \gg 1 \tag{3}$$

where $G^{(1)}$ the gain in the first ondulator (modulator), $P_{in}^{(2)}$ is the power at the entrance of the second ondulator (radiator), and P_{shot} the effective power of shot noise in the electron beam.

Since the incoming SASE-FEL radiation is formed by short duration pulses (a set of spikes with a temporal envelop of a few femtoseconds, FWHM), the problem of dynamical reflection by unpatterned and patterned multilayers is considered in section 3.

2. X-FEL self-seeding with Bragg reflectors in double-crystal non-dispersive configuration and backscattering geometry

To argument our proposal of using Bragg multilayer mirrors for the monochromator, we must quantify the problem on the basis of actual performances of these optical devices.

To fix the problem, we will consider Bragg multilayer mirrors developed for extreme UV (EUV) lithography since owing to their interest, these optics have been considerably developed and are well documented. We consider the case of multilayer optics at $\lambda \sim 6.6/6.7\ nm$ designed for the next generation of EUV lithography. At the wavelength of $6.65\ nm$, it is measured [6] for a La/B multilayer mirror, a relative wavelength width $\frac{\Delta\lambda}{\lambda}$ around $\frac{0.05nm}{6.67nm} \approx 0.8\ \%$ for $\theta_B = 88.5°$ (not far away from the normal incidence) with a peak reflectivity around 64 %.

If we identify this value of $\frac{\Delta\lambda}{\lambda}$ with $\mathcal{R}_m$ and consider a typical value of $\mathcal{R}_{SASE}$ about 0.5 %, it follows that $K_s \sim 2$. It seems that this result may hinder our proposal. But different arguments may lead to a more optimistic conclusion because we can envisage at least three ways to improve $\mathcal{R}_m$: backscattering geometry, use of patterned mirror and detuning of the double-crystal monochromator.

To ensure, in the soft x-ray domain, the monochromatization needed for the self-seeding, we suggest the use of Bragg multilayer reflectors in the near backscattering or near-normal incidence geometry (*i.e.* Bragg angle close to $\frac{\pi}{2}$) in a double-crystal non-dispersive configuration (see figure 2).

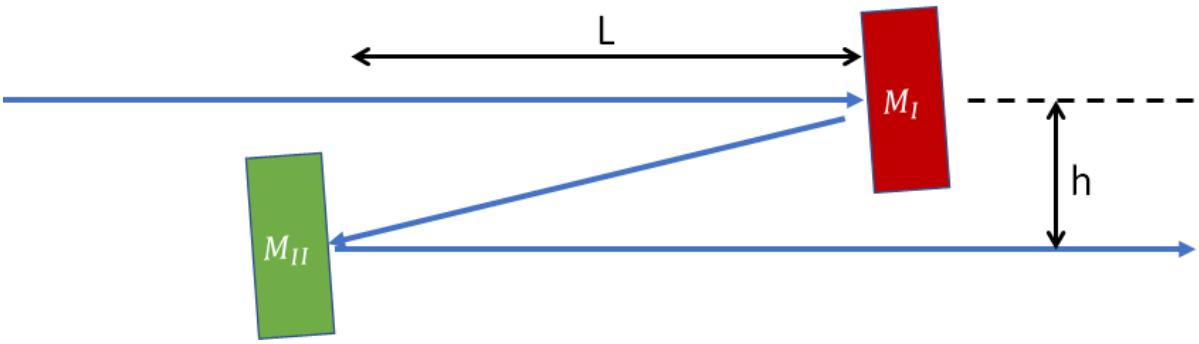

Figure 2 : Double-multilayer monochromator in non-dispersive configuration and in near backscattering geometry. M_I is an unpatterned multilayer; M_{II} is a patterned multilayer. L is the distance between the two multilayers; h is the distance between the incoming and outgoing parallel beams.

Under backscattering geometry, the diffraction spectral band becomes very narrow and this geometry offers the possibility of high resolution compared to grazing scheme which is necessary to satisfy criterion given by Eq.(1). A first reason for this behavior can be easily found by differentiating the Bragg law :

$$2\, d_p\, sin\theta = p\, \lambda$$

(4)

where λ is the radiation wavelength in vacuum, p an integer called diffraction order, d_p the effective d-spacing[1] depending on the order p and on the average refractive index $\bar{n}$ of the multilayer structure and θ the glancing angle. Differentiation gives :

$$\frac{\Delta\lambda}{\lambda} = \frac{\Delta d_p}{d_p} + cotan\theta\, \Delta\theta$$

(5)

The quantity $\frac{\Delta\lambda}{\lambda}$ is the relative width of the wavelength band, Δd_p is a variation of the effective d-spacing resulting from various possible causes (mechanical strain, thermal load, …). From Eq. (5), it appears that under backscattering geometry, $cotan\theta \approx 0$ since $\theta \approx \frac{\pi}{2}$ and that $\frac{\Delta\lambda}{\lambda}$ becomes independent of the angular spread $\Delta\theta$. This latter quantity needs some precision ; it is generally conditioned both by the beam divergence ψ and the angular width ω^θ of the monochromator diffraction pattern.

Assuming Gaussian distributions, we add in quadrature and get :

$$\Delta\theta \approx \sqrt{(\omega^\theta)^2 + \psi^2}$$

(6)

Let us emphasize that for X-FEL radiation, the divergence ψ is a few microradians while the angular width ω^θ is a few milliradians so that $\ll \omega^\theta$ and $\Delta\theta \approx \omega^\theta$. In case of a crystal, ω^θ is often associated with the Darwin angular width ω_D. For a multilayer diffracting in the soft x-ray range where photo-absorption is generally important, Darwin dynamical theory is not well suited. Nevertheless, we assume that the Darwin model can be usefully considered for our heuristic approach. For $\theta < \frac{\pi}{2}$, ω_D is given for a Bragg symmetric diffraction by :

$$\omega_D = \frac{2\,|C\,\chi|}{sin\,2\,\theta}$$

(7)

where χ is the Fourier component of the dielectric susceptibility and C a polarization-dependant term close to 1 in backscattering geometry.

[1] The subscript p in d_p corresponds to the fact that the effective d-spacing is not the geometrical distance but rather the optical one taking into account optical effects (refraction and absorption) ; the optical effects depend on the order p ; when p tends towards infinty the effective d-spacing tends towards the geometrical distance d_∞.

In case of a multilayer structure formed with bilayers made up with materials **a** and **b** the thickness of which are $d_{\mathbf{a}}$ and $d_{\mathbf{b}}$ and the optical indices are $n_{\mathbf{a}} = 1 - \delta_{\mathbf{a}} + i\,\beta_{\mathbf{a}}$ and $n_{\mathbf{b}} = 1 - \delta_{\mathbf{b}} + i\,\beta_{\mathbf{b}}$ respectively, then :

$$\chi = -\frac{i}{\pi}\,(\delta_{\mathbf{a}} - \delta_{\mathbf{b}})\,F(\gamma, p) \tag{8.1}$$

where

$$F(\gamma, p) = \frac{1}{p}\,[1 - \exp(2\pi\, i\, p\, \gamma)]\,, \gamma = \frac{d_{\mathbf{a}}}{d_{\mathbf{a}} + d_{\mathbf{b}}} \tag{8.2}$$

Since $\chi \propto \lambda^2$, taking into account the Bragg law, it follows that ω_D increases as $tan\theta$ with increasing θ. Nevertheless in the backscattering geometry, an anomalous effect occurs [7–10] and it can be shown that :

$$\omega^{\theta} = 2\sqrt{|\,\chi|} \tag{9.1}$$

and the spectral width in terms of wavelength ω^{λ} is linked to ω^{θ} :

$$\omega^{\lambda} = \frac{1}{4}\left(\omega^{\theta}\right)^2 \tag{9.2}$$

which means that a considerable increase of the angular width and consequently of the luminosity, occurs.

For crystals, Eqs. (9) are valid for near backscattering geometry provided the Bragg angle deviates from $\frac{\pi}{2}$ only by approximately ω^{θ}. We call this case, the near-backscattering regime. To our knowledge, this regime has not been considered nor documented in case of diffraction by a multilayer structure in the soft-x-ray domain where photo-absorption dominates except in [11] where a formula similar to (9.2) is proposed. Even in this regime, it is needed to reduce the value of ω^{θ} because the exact backscattering is not possible and one has to reduce the product $cotan\theta\ \omega^{\theta}$ to diminish $\frac{\Delta\lambda}{\lambda}$, see Eq. (5). For $\theta = 89.5°$ taking $\omega^{\theta} \approx 10^{-2}$ rad, we can expect $\frac{\Delta\lambda}{\lambda} \approx cotan\theta\ \omega^{\theta}$ around 10^{-4} since $cotan\theta \approx 9\ 10^{-3}$ if the term $\frac{\Delta d_p}{d_p}$ can be neglected. Let us note that the value $\theta = 89.5°$ seems reasonable since it leads to $h \approx 5\ mm$ for $L \approx 50\ cm$, see figure 2.

Another reason for the choice of the backscattering geometry concerns the penetration of the radiation : the larger the number of bilayers N_{diff} involved in the diffraction process, the narrower the bandwidth of the diffracted radiation. In the soft x-ray domain, photo-absorption is often the main cause for the limited penetration. The penetration depth (the depth into the material measured along the surface normal) D is linked to the penetration length L by $D = L\,sin\,\theta$. Increasing the value of D leads to the rise of N_{diff}. Since $L \sim 1/\bar{\mu}$ where $\bar{\mu}$ is the average linear absorption coefficient of the multilayer medium, it comes :

$$D \sim 1/\bar{\mu}\ sin\,\theta \tag{10}$$

In backscattering geometry, $\theta \approx \frac{\pi}{2}$ and then the penetration depth D is maximized. From Eq. (10), it appears that another way to increases D is to diminish the value of $\bar{\mu}$. To do, we propose to lighten the medium as explained below.

Using a patterned multilayer mirror as monochromator is an efficient way to increase the penetration depth D. Indeed, according to Eq. (10) if the absorption coefficient $\bar{\mu}$ becomes smaller, D is augmented. Etching the multilayer structure allows to lighten the structure by adding empty spaces (the grooves) and consequently it allows one to diminish the value of $\bar{\mu}$. It has been shown that etching according to a laminar profile (see figure 3) leads to an important narrowing of the bandwidth provided that the parameters (numbers of bilayers, grating period D_G, filling factor Γ, ...) are judiciously chosen [12,13]. Such patterned mirrors have been realized and successfully tested in the soft x-ray domain [14,15]. A reduction of the bandwidth by a factor $1/\Gamma$ can be obtained without large loss of reflectivity. To do it, a value of Γ lower than 0.2 is generally prohibited. Also, taking Γ~0.25 allows a bandwith reduction by a factor 4 with respect to the unpatterned mirror.

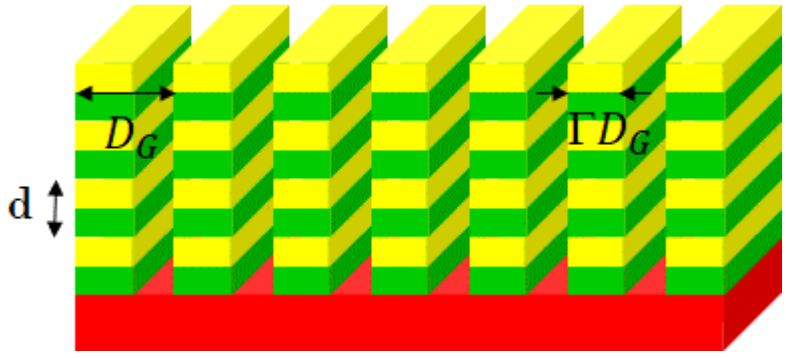

Figure 3 : Multilayer mirror patterned under lamellar profile. D_G is the grating period; ΓD_G is the width of the multilayer bars; d is the multilayer period or d-spacing.

We then propose to combine the backscattering geometry along with the use of unpatterned and patterned mirrors in a detuned double-crystal non-dispersive configuration to form a monochomator system, according to a layout shown in figure 2. We call this set-up double-multilayer detuned monochromator or DMDM. The first monochromator M_I, with a period d_I, is an unpatterned mirror ensuring the maximal collection of the photon flux coming the first ondulator (modulator), while the second monochromator M_{II} with a period d_{II} chosen different from d_I to allow the detuning (see below), is a patterned mirror. The detuning consists in performing a spectral shift of the diffraction patterns of the monochromators I and II with a partial overlapping according to the principle illustrated by figure 4. By detuning, it is possible to reduce $\frac{\Delta\lambda}{\lambda}$ by a factor 4 without large loss of peak reflectivity.

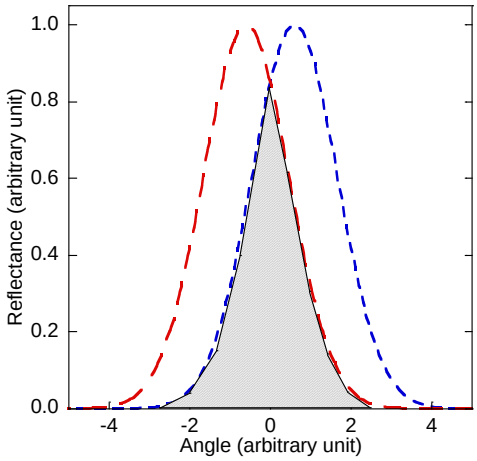

Figure 4 : Detuning of the multilayer monochromators of the DMDM. The dashed zone corresponds to the overlap of the diffraction patterns of the patterned and unpatterned multilayers.

With natural crystals, this detuning operation is generally performed by tilting the second monochromator M_{II} so that the beam impinges M_{II} with a different angle from the one on monochromator M_I. In this case, the outgoing beam is not parallel to the incoming one. With artificial Bragg monochromators, it is possible to draw advantages from the freedom in the choice of the parameters. It is feasible to modify the d-spacing,

and then to change d_{II} with respect to d_I, while keeping the same incident angle. In this case, parallelism is kept which considerably simplifies the experimental layout.

The combined effects of refraction and absorption lead to an optical shift of wavelength $D\lambda$ with respect the value of the Bragg wavelength λ_B given by $\lambda_B = 2d_\infty$ in backscattering geometry. For monochromators I and II with the same d-spacing ($d_{I\infty} = d_{II\infty} = d_\infty$), the wavelength shift $D\lambda$ is only due to optical (dispersion and absorption) effect and identifies with the quantity $\delta\lambda_{op}$ given in Appendix 1 on the basis of the work by Rosenbluth and Lee [16]. In this case, if we take the following typical values : $\Gamma = 0.25$, $\gamma = 0.3$ and $\bar{\delta} = 86\ 10^{-4}, \bar{\beta} = 7\ 10^{-4}, \Delta\delta_I = 194\ 10^{-4}, \Delta\beta_I = 9\ 10^{-4}$ for the example considered previously [6]; $|\delta\lambda_{op}|$~0.033 nm at the wavelength equal to 6.65 nm and with $d_\infty = 3.32\ nm, \Gamma = 0.25$.

The values of the optical indices come from [17]. Taking into account that the measured wavelength bandwidth $\Delta\lambda$ is around 0.05 nm for the example considered previously [6], the wavelength detuning shift $\delta\lambda_{op}$ associated with the optical term seems in agreement with the expected detuning $\frac{\Delta\lambda_I}{2}$ (≈ 0.025 nm), $\Delta\lambda_I$ being the wavelength bandwidth of monochromator M_I. Anyway, it is possible to adjust the value of $\delta d_{I,II\infty}$ to get the wavelength detuning $\delta\lambda$ at the wished value $\frac{\Delta\lambda_I}{2}$.

To sum up, backscattering geometry permits an enhancement of luminosity and an improvement of resolution associated with a cancellation of the angular spread and with a rise of the incident penetration depth. Detuning by a modification of the d-spacing (and not a tilt of one monochromator) ensures an improvement of the monochromator resolution while keeping the parallelism between the incoming and outgoing beams.

The choice of the materials of the multilayer structures is also important : of course, one wishes to find the best couple of materials to achieve the largest peak reflectivity of the monochromator but also to obtain simultaneously the narrower spectral bandwidth. Reaching these two goals simultaneously may be tricky since it has been shown that increasing the reflection coefficient of a unit-cell (*i.e.* a bilayer) and consequently the overall reflectivity of a multilayer reflector, tends to increase the bandwidth [18].

A degradation of resolution and a spectral shift may result from variations of layer thicknesses Δd_p around their nominal value. As mentioned previously, Δd_p can arise from mechanical or thermal influences but in the case of multilayer structures, may also come from errors in the thicknesses during the deposition for various technical reasons.

In fact the more critical point is the thermal loading (see section 4). Decrease in resolution can also result from interfacial roughness. The influence of geometrical or chemical roughness on the bandwidth has been investigated [19].

3. Discussion of the Feldhaus criterion

By combining the three methods (backscattering geometry, use of patterned mirror and detuning), a reduction of the bandwidth by a factor 20 with respect to a mere unpatterned mirror working in non-backscattering geometry can be expected with an acceptable loss of the global throughput of the DMDM. Consequently it seems possible to achieve $\mathcal{R}_m \approx 10^{-4}$ and then $K_s = \frac{\mathcal{R}_m}{\mathcal{R}_{sase}} \approx \frac{10^{-4}}{5\ 10^{-3}} = 2\ 10^{-2}$ so that the criterion given by Eq. (1) is satisfied.

Taking into account that the average value of the length of the electron bunch σ_z is around 50 μm, the quantity $\frac{\lambda}{\pi\ \sigma_z}$ is around 4 10^{-5} at the wavelength of interest, and then the criterion given by Eq. (2) is also satisfied. Concerning the criterion given by Eq. (3), the transmission factor T_m and hence R_m must be evaluted. The integral reflection coefficient R_m of the DMDM denoted R_{DMDM}, can be expressed as follows by means of the peak reflectivity of each monochomator R_{Mi}^P $(i = I/II)$:

$$R_{DMDM} = P\ R_{MI}^P R_{MII}^P \tag{11}$$

The factor P depends largely on the rate of overlapping in the detuning process. With the assumption of diffraction patterns with a Gaussian profile, it is possible to get a coarse estimation of a value of P (see Appendix 2) :

$$P \approx \sqrt{\pi}\ \exp\left[\frac{-(\delta\lambda)^2}{{\sigma_I}^2 + {\sigma_{II}}^2}\right] \tag{12.1}$$

with :

$$\sigma_i = \frac{\Delta\lambda_i}{2\sqrt{Ln2}} \tag{12.2}$$

$\Delta\lambda_i$ being the FWHM of the Gaussian profile of the diffraction pattern of the monochromator i and $\delta\lambda$ the detuning wavelength shift. If one assumes that $\Delta\lambda_{II} = \Gamma\ \Delta\lambda_I, \Gamma < 1$, by virtue of the use of an etched mirror, and that the wavelength shift $\delta\lambda$

associated with the detuning is only a part of the bandwidth $\Delta\lambda_I : \delta\lambda = g\,\Delta\lambda_I, g < 1$, then :

$$\frac{(\delta\lambda)^2}{{\sigma_I}^2 + {\sigma_{II}}^2} = \frac{4\,Ln2\;g^2}{1+\Gamma^2} \tag{13.1}$$

$$P \approx \sqrt{\pi}\;\exp\left[-\frac{4\,Ln2\;g^2}{1+\Gamma^2}\right] \tag{13.2}$$

For $\Gamma = 0.25, g = 0.5$ then $\exp\left[\frac{-(\delta\lambda)^2}{{\sigma_I}^2+{\sigma_{II}}^2}\right] \approx 0.521$ and $P \approx 0.923$.

One defines $T_m = T_{DMDM}$ as the product of the integral reflection coefficient R_{DMDM} of the DMDM with the coefficient K_s :

$$T_{DMDM} = K_s\,R_{DMDM} \tag{14}$$

where K_s describes the radiation loss at the exit of the DMDM. This quantity must be sufficiently large to satisfy the criterion given in Eq. (3). In the practical case under consideration, $R_{MI}^P \approx 0.6, R_{MII}^P \approx 0.8\,R_{MI}^P, R_{DMDM} = P\,R_{MI}^P R_{MII}^P \approx 0.265$, so that, with $K_s \approx 2\;10^{-2} : T_{DMDM} \approx 53\;10^{-4}$. It results that $G^{(1)}\,T_{DMDM} \approx 530$ and the criterion given by Eq. (3) is satisfied. As emphasized in [1], there is an upper limit on the value of the gain $G^{(1)}$ given by the limit of the heat load that the monochromator can withstand.

To summarize, it seems possible to fulfil all the criteria given Ref. [1], by means of appropriate Bragg reflectors working in double-crystal non-dispersive configuration and backscattering geometry.

4. Dynamics of the monochromatization and of self-seeding

4.1 Reflection in the time-domain

Since the SASE-XFEL radiation consists in a train of femtosecond pulses enveloping spikes (a tenth of fs) randomly distributed within the envelop, the temporal aspect of the diffraction cannot be ignored. It is not possible to consider the FEL radiation as a plane wave whose propagation can be treated in the frequency domain. The temporal dynamics of diffraction has been investigated in case of crystal reflection through different approaches (Fourier transform, Tagaki-Taupin, …) [20,21].

In case of multilayer mirrors, the subject has been treated directly in the time domain using the matricial method [22, 23]. The case of a patterned reflector with a laminar profile as shown in figure 2 can be reduced to the one of the unpatterned mirror with a sufficient accuracy in the specular reflection case, provided that one multiplies the value of the susceptibility of each material by the factor Γ.

It is assumed that the intensity of the X-FEL radiation at the exit of the modulator is low enough so that non-linear effects do not occur : it is the low-intensity regime, LIR. Nevertheless, even if the response of the mirror to the pulse is then purely linear in LIR, notable effects occur when the time-width of the pulse is very short. It has been shown [23] that under the incidence of a Dirac pulse, the diffracted field can be written by means of the Bessel function of the first kind J_1 :

$$\mathcal{E}_-(z=0,T)_{\text{Dirac}} \;=\; i\,sin\theta\;K^-\;\frac{\Lambda}{\pi\sqrt{2\pi}}\frac{J_1[\zeta(T)]}{\zeta(T)}\Theta(T)\;;\;\zeta(T)=\frac{\pi}{\Lambda}\,sin\theta\;c\;T \tag{15}$$

One has introduced the time delay T measured with respect to the diffracted wave plane:

$$T=\frac{c\;t-\;x\;cos\;\theta}{c} \tag{16}$$

and a length Λ ,which corresponds to the extinction length in the dynamical theory of crystal diffraction, given in the case of diffraction by Bragg artificial reflectors (unpatterned or patterned mirrors) by :

$$\Lambda^2=\;-\frac{\pi^2}{K^+K^-} \tag{17.1}$$

where :

$$K^+=-\;\frac{k}{sin\theta}\;2\pi\;\Delta\chi\;u_p$$
$$K^-=\;\frac{k}{sin\theta}2\pi\;\Delta\chi\;u_{-p} \tag{17.2}$$

The terms $\Delta\chi$ and u_p are given by the Fourier expansion of the $\chi(z)$ profile of the multilayer reflector :

$$\chi(z) = \bar{\chi} + \sum_{p=-\infty}^{+\infty} \Delta\chi \; u_p \, e^{i\,pg\,z} \;, g = \frac{2\pi}{d} \tag{18}$$

For a bilayered system :

$$u_p = \gamma \, \mathrm{sinc}(\pi p \gamma) \, e^{-i\pi p \gamma} \tag{19}$$

In exact backscattering geometry, the time delay T and the time t are merged. The term $\frac{J_1[\zeta(T)]}{\zeta(T)}$ gives the profile of the wake field. As shown in figure 5, this profile oscillates and presents N maxima which correspond to the zeros of the Bessel function J_1. The position of the j^{th} maximum is denote by T_j. One inherent problem with the Bragg diffraction is that the outgoing beam seeding the radiator exhibits a transverse shift in position. It can be shown that this phenomenon is attenuated for near perpendicular incidence [24] which advocates once more for the (near) Bragg scattering geometry.

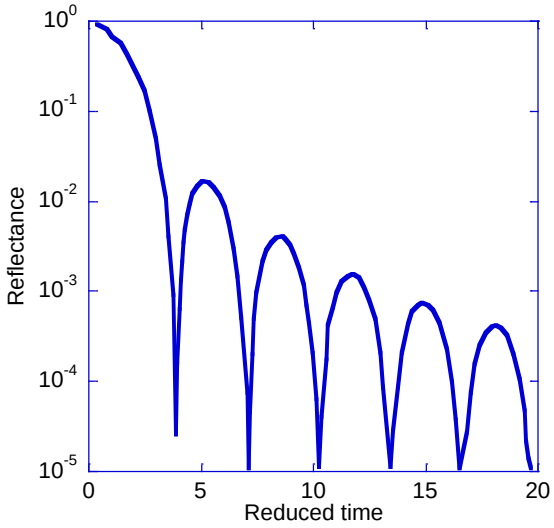

Figure 5 : Temporal profile of the Bragg reflected wave as a function of reduced time $\bar{t} = t \; sin\theta \, \frac{\pi \, c}{\Lambda}$.

The preceding results agree with those given by Lindberg and Shvydd'ko [24, 25] for the self-seeding method based on diffraction by a crystal for the hard x-ray domain. The short temporal width of the SASE-XFEL pulses can be a source of problem linked to a loss of efficiency of the Bragg reflector as shown hereafter. First, we consider $\hat{R}_\delta(T) = \mathcal{E}_-(z=0,T)_{\mathrm{Dirac}}$ the impulse response in terms of reflection which is nothing else than

the temporal Green function $g_R(T)$ for reflection [23] and is given by Eq. [15]. For time coherent radiation with time-dependent causal distribution Ξ (normalized to unity), the indicial response $\hat{R}_\Theta(t)$ in terms of reflection coefficient is then given by :

$$\hat{R}_\Theta(t) = \int_{-\infty}^{+\infty} |g_R(T)|^2 \, \Xi(t-T)\, dT = \int_0^t \left|\hat{R}_\delta(T)\right|^2 \Xi(t-T)\, dT \tag{19}$$

Eq. (19) allows one to draw a "universal" curve in terms of peak reflectance for the indicial response $\hat{R}_\Theta(t)$ versus the reduced time $\bar{t} = t\, sin\theta \frac{\pi\, c}{\Lambda}$; see figure 6. It appears that the indicial response for reflection is conditioned by the extinction length Λ and that it presents a transient period whose duration is given by a characteristic transient time t_c approximately equal to 2 units of reduced time.

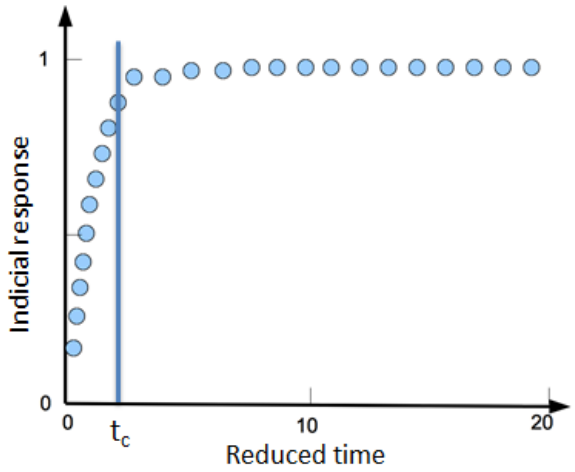

Figure 6 : Indicial response in terms of peak reflectance versus reduced time for a multilayer mirror at the Bragg resonance (Bragg angle). The response is normalized to unity. The effect of the oscillations of the wake field can be observed at $\bar{t} = T_1 \approx 3.83$.

From the indicial responses of the multilayer reflector, it is possible to calculate the time-dependent reflection of a given short pulse. Let $I(t)$ be the temporal envelope shape of any incident pulse and *O(t)* the envelope of the corresponding reflected pulse. Then the Laplace transform $O(s)$ of *O(t)* is related to the Laplace transform $I(s)$ of $I(t)$ by means of the convolution theorem :

$$O(s) = \hat{Z}_\delta(s)\, I(s) \tag{20}$$

$\hat{Z}_\delta(s)$ being the transfer function that is the Laplace transform of the impulse response $\hat{Z}_\delta(t) \equiv \hat{R}_\delta(t)$; $\hat{Z}_\delta(t)$ can be determined from $\hat{Z}_\Theta(t)$ and then by performing an inverse

Laplace transform of Eq. (20), one determines the temporal response [22]. This approach is applied to a sine-square shaped pulse with 10 fs temporal width reflected by an ideal La/B multilayer mirror working in backscattering geometry, as illustrated by figure 7. The multilayer mirror has a period equal to $d_\infty = 3.32$ nm, a ratio $\gamma = 0.3$ and 150 bilayers. It appears that, although the mirror offers a steady-time peak reflectivity around 64 %, the intensity of the reflected pulse is considerably reduced and has a temporal shape notably modified with respect to the incident pulse.

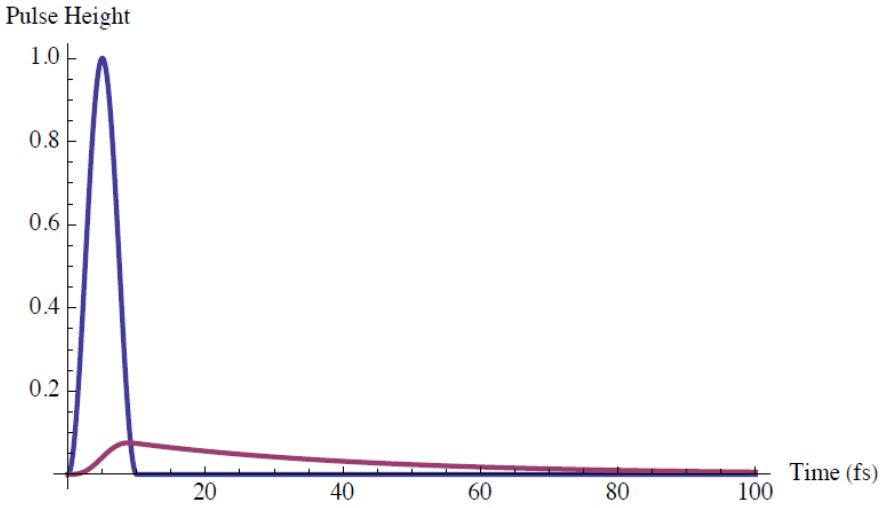

Figure 7 : Normalized incident sine-square shaped pulse (blue curve) and reflected pulse by a La/B multilayer working at the wavelength 6.65 nm in backscattering geometry vs time (red curve).

Although the problem of reduction in reflection efficiency for an x-ray reflector, at reduced time less than the critical time t_c has been highlighted in 1995 by Chuhovskii and Förster for crystal diffraction [25] and then by André and Jonnard [22,23] for multilayer diffraction, it seems that this effect is little considered in the literature relative to XFEL optics.

4.2 Dynamics of the self-seeding

In the preceding section, we discussed the spatio-temporal profile of the radiation reflected by the DMDM generated by a coherent incident pulse. But since the SASE-XFEL radiation impinging the DMDM is temporally incoherent, we now discuss the dynamics to seed coherently the second ondulator (radiator). The SASE-XFEL is approximately constituted by *N* longitudinal Gaussian modes that have random phases. So we write the incoming field :

$$E_{inc}(t) = \mathcal{E}(t) \sum_{i=1}^{N} \frac{\vartheta_i \, exp\left(-\frac{c^2 \Delta t_i}{4\,\sigma}\right)}{\sigma\sqrt{4\,\pi}} \tag{21}$$

where ϑ_i is a set of random amplitudes, Δt_i a set of random temporal shifts, σ the width of the temporal random distribution, $\mathcal{E}(t)$ the temporal envelope of the incident field caracterized by a characteristic length $L_{SASEpulse}$. Provided the incident pulse is short enough, it generates a trailing field formed by a sum of wakes as shown in the previous section, each of them with an amplitude ϑ_i and a temporal shift Δt_i. If the ensemble-averaged total power in the trailing pulse scales as N times the average power in an individual wake, then we can write the ratio of the seeding power P_{seed} to the SASE-XFEL pulse power P_{pulse} as :

$$\frac{P_{seed}}{P_{SASEpulse}} = 4\pi\sigma\, N\left(\frac{\pi^2}{\Lambda^2}\frac{d}{}\frac{J_1[\zeta(T_1)]}{\zeta(T_1)}\right) \tag{22}$$

where T_1 is the delay time corresponding to the first maximum in $\frac{J_1[\zeta(T)]}{\zeta(T)}$.

For a long modulator acting on an electron beam with zero initial energy spread, one has $\sigma = L_{SASE}/\sqrt{3\pi}$; moreover $N = L_{SASEpulse}/L_{coh}$. Combining these relations gives the approximate formula :

$$\mathcal{R}_{s;p} \equiv \frac{P_{seed}}{P_{SASEpulse}} \approx L_{SASE}\, L_{coh}\left(\frac{\pi^2}{\Lambda^2}\frac{d}{}\frac{J_1[\zeta(T_1)]}{\zeta(T_1)}\right) \sim \frac{L_{SASEpulse}\, L_{coh}}{(cT_1)^2} \tag{23}$$

It appears that the ratio $\mathcal{R}_{s;p}$ is mainly conditionned by the value of T_1 as pointed out by Shvydd'ko and Lindberg for the crystal diffraction case [26]. To optimize the seeding, it is then worth to increase the value of T_1 ; since this quantity varies as $sin\theta$, it follows that backscattering is a favorable geometry. Increase the value of T_1 is also determined by a judicious choice of the materials from which the structure of the multilayer reflectors is made up.

4. Conclusion

A double-crystal monochromator in non-dispersive configuration equipped with multilayered Bragg reflectors working in near backscattering geometry appears to be a

powerful tool for performing self-seeding in a soft-x-ray FEL. To achieve a sufficient performance in terms of monochromatization, one of this Bragg reflector should be an etched structure which allows one to improve notably the resolution of a multilayer mirror. One of the main problems to solve is the damages in the x-ray beam transport system arising from the head load resulting from the interaction X-FEL radiation with the matter. Since the self-seeding system is exposed to the radiation coming from the modulator, one can expect that this damage problem is less acute than the one arising for optics installed after the radiator. The problem of thermal loading on La/B multilayer mirrors is not well documented. Nevertheless for B-based mirrors such as La/B_4C or LaN/B_4C systems also of interest in the B-K spectral domain, structural modifications and interfacial chemical reactions have been evidenced leading to spectral shift in the reflectivity curve under annealing [27]. At the exit of a modulator, a typical energy over pulse of a few μJ (say 4 µJ) is expected which corresponds, for a *rms* spot size of 50 µm, to a fluence of 200-300 mJ/cm^2 which seems compatible with the stability of the mirrors [28]. Nevertheless both theoretical and experimental investigations are needed to corroborate this with the B-based multilayer systems of interest, in the B-K spectral domain. Multi-scale and multi-physics numerical models in this field are now available [29] but required to be validated by experiments. Another question is linked to the short-duration of the radiation pulses. It has been theoretically shown that the reflectivity of the mirrors can be affected by the temporal features of the pulse radiation. Until now, no validation of the theory of the diffraction dynamics has been obtained and experiments in this field should be performed to check theory.

Appendix 1

Following the work by Rosenbluth and Lee [16], for a bilayer structure as considered in Eq. (8), $D\lambda$ is given by :

$$D\lambda = \lambda - \lambda_B = 2d_\infty \, \epsilon\left(\bar{\delta}, \bar{\beta}, \Delta\delta, \Delta\beta\right) \tag{A1.1}$$

where $\epsilon\left(\bar{\delta}, \bar{\beta}, \Delta\delta, \Delta\beta\right)$ is a function of :

- the average unit decrement of the real part of the optical index $\bar{\delta} = \gamma \, \delta_{\mathbf{a}} + (1 - \gamma)\delta_{\mathbf{b}}$;
- the average of the imaginary part of the optical index $\bar{\beta} = \gamma \, \beta_{\mathbf{a}} + (1 - \gamma)\beta_{\mathbf{b}}$;
- the difference between the real parts of the optical index $\Delta\delta = \delta_{\mathbf{a}} - \delta_{\mathbf{b}}$ of the two materials;
- the difference between the imaginary parts of the optical index $\Delta\beta = \beta_{\mathbf{a}} - \beta_{\mathbf{b}}$ of the two materials.

From [16], it comes with the usual notations of the paper :

$$\epsilon\left(\bar{\delta}, \bar{\beta}, \Delta\delta, \Delta\beta\right) = \bar{\delta} - \frac{\Delta\delta \, \Delta\beta \, sin^2(p \, \gamma\pi)}{\bar{\beta} \, (p \, \pi)^2} \tag{A1.2}$$

Applying Eq. (A1.1) to the monochromator I leads to :

$$\lambda_I = 2d_{I\infty} \left[1 + \epsilon\left(\bar{\delta}_I, \bar{\beta}_I, \Delta\delta_I, \Delta\beta_I\right)\right] \tag{A1.3}$$

where the subscript I refers to monochromator I. The same operation can be applied *mutatis mutandis* to monochromator II, so that the wavelength shift $\delta\lambda$ resulting from the detuning reads :

$$\delta\lambda \equiv \lambda_I - \lambda_{II} = 2d_{I\infty} \left[1 + \epsilon\left(\bar{\delta}_I, \bar{\beta}_I, \Delta\delta_I, \Delta\beta_I\right)\right] - 2d_{II\infty} \left[1 + \epsilon\left(\bar{\delta}_{II}, \bar{\beta}_{II}, \Delta\delta_{II}, \Delta\beta_{II}\right)\right] \tag{A1.4}$$

which can be rewritten as :

$$\delta\lambda = 2\delta d_{I,II\infty} + \left(2d_{I\infty}\epsilon\left(\bar{\delta}_I, \bar{\beta}_I, \Delta\delta_I, \Delta\beta_I\right) - 2d_{II\infty}\epsilon\left(\bar{\delta}_{II}, \bar{\beta}_{II}, \Delta\delta_{II}, \Delta\beta_{II}\right)\right) \tag{A1.5}$$

where

$$\delta d_{I,II\infty} = d_{I\infty} - d_{II\infty} \tag{A1.6}$$

For monochromators I and II with the same d-spacing $d_{I\infty} = d_{II\infty} = d_{\infty}$, then $\delta d_{I,II\infty} = 0$, and the wavelength shift is only due to optical (dispersion and absorption) effect :

$$\delta\lambda_{op} = 2d_{\infty}\left(\epsilon\left(\bar{\delta}_I, \bar{\beta}_I, \Delta\delta_I, \Delta\beta_I\right) - \epsilon\left(\bar{\delta}_{II}, \bar{\beta}_{II}, \Delta\delta_{II}, \Delta\beta_{II}\right)\right) = 2d_{\infty}\epsilon\left(\bar{\delta}_I, \bar{\beta}_I, \Delta\delta_I, \Delta\beta_I\right)(1-\Gamma) \quad \text{(A1.7)}$$

Appendix 2

The integrated reflectivity of the DMDM is given by :

$$I = \int_{-\infty}^{+\infty} R_{peak\ /MI} \exp\left[-\frac{(\lambda-\lambda_I)^2}{{\sigma_I}^2}\right] R_{peak\ /MII}\ \exp\left[-\frac{\left(\lambda-(\lambda_I \pm \delta\lambda)\right)^2}{{\sigma_{II}}^2}\right] d\lambda \tag{A2.1}$$

If one sets $x = (\lambda - \lambda_I)$ then :

$$I = R_{peak\ /MI}\ R_{peak\ /MII} \int_{-\infty}^{+\infty} \exp\left[-\frac{x^2}{{\sigma_I}^2}\right] \exp\left[-\frac{(x \mp \delta\lambda)^2}{{\sigma_{II}}^2}\right] dx \tag{A2.2}$$

The integral can be rewritten as follows :

$$\exp\left[-\frac{(\delta\lambda)^2}{{\sigma_{II}}^2}\right] \int_{-\infty}^{+\infty} \exp\left[-\frac{x^2}{\bar{\sigma}^2}\right] \exp\left[-\frac{\mp 2\, x\, \delta\lambda}{{\sigma_{II}}^2}\right] dx \tag{A2.3}$$

where :

$$\frac{1}{\bar{\sigma}^2} = \frac{1}{{\sigma_I}^2} + \frac{1}{{\sigma_{II}}^2} = \frac{{\sigma_I}^2 + {\sigma_{II}}^2}{{\sigma_I}^2 {\sigma_{II}}^2} \tag{A2.4}$$

Since :

$$\int_{-\infty}^{+\infty} \exp(-\alpha\, x^2 \pm \beta\, x)\ dx = \sqrt{\frac{\pi}{\alpha}} \exp\left(\frac{\beta^2}{4\alpha}\right) \tag{A2.5}$$

it comes :

$$I = R_{peak\ /MI}\ R_{peak\ /MII} \sqrt{\pi}\, \bar{\sigma}\ \exp\left[-\frac{(\delta\lambda)^2}{{\sigma_{II}}^2}\right] \exp\left(\frac{\bar{\sigma}^2\,(\delta\lambda)^2}{{\sigma_{II}}^4}\right)$$

$$= R_{peak\ /MI}\ R_{peak\ /MII} \sqrt{\pi}\, \bar{\sigma}\ \exp\left[\frac{-(\delta\lambda)^2}{{\sigma_I}^2 + {\sigma_{II}}^2}\right] \tag{A2.6}$$

To obtain the dimensionless P factor in agreement with the definition, one divides I by $\bar{\sigma}$ $R_{peak\ /MI}\ R_{peak\ /MII}$ so that :

$$P = \sqrt{\pi}\ \exp\left[\frac{-(\delta\lambda)^2}{{\sigma_I}^2 + {\sigma_{II}}^2}\right] \tag{A2.7}$$

References

[1] J. Feldhaus, E. L. Saldin, J. R. Schneider, E. A. Schneidmiller, and M. V. Yurkov, *Possible Application of X-Ray Optical Elements for Reducing the Spectral Bandwidth of an X-Ray SASE FEL*, Opt. Commun. **140**, 341 (1997).

[2] E. L. Saldin, E. A. Schneidmiller, Yu. V. Shvyd'ko, and M. V. Yurkov, *X-Ray FEL with a MeV Bandwidth*, Nucl. Instrum. Methods Phys. Res. Sect. Accel. Spectrometers Detect. Assoc. Equip. **475**, 357 (2001).

[3] G. Geloni, V. Kocharyan, and E. Saldin, *A Novel Self-Seeding Scheme for Hard X-Ray FELs*, J. Mod. Opt. **58**, 1391 (2011).

[4] G. Geloni, *Self-Seeded Free-Electron Lasers*, in *Synchrotron Light Sources and Free-Electron Lasers: Accelerator Physics, Instrumentation and Science Applications*, edited by E. J. Jaeschke, S. Khan, J. R. Schneider, and J. B. Hastings (Springer International Publishing, Cham, 2016), pp. 161–193.

[5] J. Amann et al., *Demonstration of Self-Seeding in a Hard-X-Ray Free-Electron Laser*, Nat. Photonics **6**, 10 (2012).

[6] D. S. Kuznetsov, A. E. Yakshin, J. M. Sturm, R. W. E. van de Kruijs, E. Louis, and F. Bijkerk, *High-Reflectance La/B-Based Multilayer Mirror for 6.x Nm Wavelength*, Opt. Lett. **40**, 3778 (2015).

[7] Y. Shvyd'ko, *X-Ray Optics*, Vol. 98 (Springer, Berlin, Heidelberg, 2004).

[8] A. Caticha and S. Caticha-Ellis, *Dynamical Theory of X-Ray Diffraction at Bragg Angles near $\pi/2$*, Phys. Rev. B **25**, 971 (1982).

[9] V. I. Kushnir and E. V. Suvovov, *Experimental Observation of a Half-Degree Angular Interval of x-Ray Reflection in Backscattering ($\theta \approx \pi/2$) from a High-Quality Crystal*, JETP Lett. **44**, 262 (1986).

[10] V. I. Kushnir and E. V. Suvorov, *X-Ray Backscattering on Perfect Crystals ($2\theta \approx \pi$)*, Phys. Status Solidi A **122**, 391 (1990).

[11] A. Rosenbluth, PhD Thesis - Reflecting Properties of x-Ray Multilayer Devices, University of Rochester, 1982.

[12] A. Sammar, J.-M. André, M. Ouahabi, B. Pardo, and R. Barchewitz, *Monochromateur multicouche à bande passante étroite pour le rayonnement X*, Comptes Rendus Académie Sci. Sér. II **316**, 1055 (1993).

[13] A. Sammar, K. Krastev, J.-M. André, R. Barchewitz, and R. Rivoira, *Narrow Bandpass Multilayer X-Ray Monochromator*, Rev. Sci. Instrum. **68**, 2969 (1997).

[14] J.-M. André et al., *X-Ray Multilayer Monochromator with Enhanced Performance*, Appl. Opt. **41**, 239 (2002).

[15] R. Benbalagh et al., *Lamellar Multilayer Amplitude Grating as Soft-X-Ray Bragg Monochromator*, Nucl. Instrum. Methods Phys. Res. Sect. Accel. Spectrometers Detect. Assoc. Equip. **541**, 590 (2005).

[16] A. E. Rosenbluth and P. Lee, *Bragg Condition in Absorbing X-ray Multilayers*, Appl. Phys. Lett. **40**, 466 (1982).

[17] *CXRO X-Ray Interactions With Matter*, http://henke.lbl.gov/optical_constants/.

[18] B. Pardo, T. Megademini, and J.-M. André, *X-UV Synthetic Interference Mirrors : Theoretical Approach*, Rev. Phys. Appliquée **23**, 1579 (1988).

[19] J.-M. André and P. Jonnard, *Photonic Bandgaps of Periodic Multilayers with Diffuse Interfaces*, J. Opt. Soc. Am. B **30**, 2296 (2013).

[20] V. A. Bushuev, *Diffraction of X-Ray Free-Electron Laser Femtosecond Pulses on Single Crystals in the Bragg and Laue Geometry*, J. Synchrotron Radiat. **15**, 495 (2008).

[21] D. Ksenzov, S. Grigorian, S. Hendel, F. Bienert, M. D. Sacher, U. Heinzmann, and U. Pietsch, *Reflection of Femtosecond Pulses from Soft X-Ray Free-Electron Laser by Periodical Multilayers*, Phys. Status Solidi A **206**, 1875 (2009).
[22] J.-M. André and P. Jonnard, *Time-Dependent Bragg Diffraction and Short-Pulse Reflection by One-Dimensional Photonic Crystals*, J. Opt. **17**, 085609 (2015).
[23] J.-M. André and P. Jonnard, *Time-Dependent Bragg Diffraction by Multilayer Gratings*, J. Opt. **18**, 015603 (2016).
[24] Y. Shvyd'ko and R. Lindberg, *Spatiotemporal Response of Crystals in X-Ray Bragg Diffraction*, Phys. Rev. Spec. Top. - Accel. Beams **15**, 100702 (2012).
[25] R. R. Lindberg and Yu. V. Shvyd'ko, *Time Dependence of Bragg Forward Scattering and Self-Seeding of Hard x-Ray Free-Electron Lasers*, Phys. Rev. Spec. Top. - Accel. Beams **15**, 050706 (2012).
[26] F. N. Chukhovskii and E. Förster, *Time-Dependent X-Ray Bragg Diffraction*, Acta Crystallogr. A **51**, 668 (1995).
[27] P. Naujok, K. Murray, S. Yulin, C. Patzig, N. Kaiser, and A. Tünnermann, *Thermal Stability of B-Based Multilayer Mirrors for next Generation Lithography*, Thin Solid Films **642**, 252 (2017).
[28] E. Louis et al., *Damage Studies of Multilayer Optics for XUV Free Electron Lasers*, Proc SPIE **7361**, 73610I (2009).
[29] F. Yang, D. L. Civita, M. Vannoni, and H. Sinn, *Damage Simulation Due to Heat Load from X-Ray FEL Beam at European XFEL*, J. Phys. Conf. Ser. **2380**, 012067 (2022).